J Membrane Biol (2010) 236:15–26
DOI 10.1007/s00232-010-9269-y

Analysis of Plasma Membrane Integrity by Fluorescent Detection of Tl^+ Uptake

Angela M. Bowman · Olena M. Nesin · Olga N. Pakhomova · Andrei G. Pakhomov

Received: 18 December 2009 / Accepted: 11 June 2010 / Published online: 11 July 2010

Abstract The exclusion of polar dyes by healthy cells is widely employed as a simple and reliable test for cell membrane integrity. However, commonly used dyes (propidium, Yo-Pro-1, trypan blue) cannot detect membrane defects which are smaller than the dye molecule itself, such as nanopores that form by exposure to ultrashort electric pulses (USEPs). Instead, here we demonstrate that opening of nanopores can be efficiently detected and studied by fluorescent measurement of Tl^+ uptake. Various mammalian cells (CHO, GH3, NG108), loaded with a Tl^+-sensitive fluorophore FluxOR™ and subjected to USEPs in a Tl^+-containing bath buffer, displayed an immediate (within <100 ms), dose-dependent surge of fluorescence. In all tested cell lines, the threshold for membrane permeabilization to Tl^+ by 600-ns USEP was at 1–2 kV/cm, and the rate of Tl^+ uptake increased linearly with increasing the electric field. The lack of concurrent entry of larger dye molecules suggested that the size of nanopores is less than 1–1.5 nm. Tested ion channel inhibitors as well as removal of the extracellular Ca^{2+} did not block the USEP effect. Addition of a Tl^+-containing buffer within less than 10 min after USEP also caused a fluorescence surge, which confirms the minutes-long lifetime of nanopores. Overall, the technique of fluorescent detection of Tl^+ uptake proved highly effective, noninvasive and sensitive for visualization and analysis of membrane defects which are too small for conventional dye uptake detection methods.

A. M. Bowman · O. M. Nesin · O. N. Pakhomova · A. G. Pakhomov (✉)
Frank Reidy Research Center for Bioelectrics, Old Dominion University, 4211 Monarch Way, Suite 320, Norfolk, VA 23508, USA
e-mail: andrei@pakhomov.net; apakhomo@odu.edu

Keywords Electroporation · Nanosecond electric pulses · Nanopores · Thallium · Cell membrane · Dye uptake · Membrane integrity

Introduction

In all living cells, the integrity of the plasma membrane is fundamentally important for maintenance of the specific intracellular milieu and support of various cell functions. Disruption of the membrane barrier function, as conveniently visualized by cell uptake of certain dye molecules, is routinely used as a simple and reliable criterion to distinguish between live and dead cells. Some of the most popular membrane integrity marker dyes, like propidium iodide (PI) and ethidium homodimer, increase the emission intensity by more than an order of magnitude upon binding to intracellular DNA and RNA, which greatly facilitates intracellular dye detection.

These dyes also proved extremely valuable for analysis and understanding of membrane disruption and resealing after electroporation (Djuzenova et al. 1996; Golzio et al. 2002; Neumann et al. 1989; Tekle et al. 1994; Weaver 2000; Zimmermann et al. 2000). The time course, magnitude and spatial distribution of dye uptake supposedly reflect the size and number of aqueous membrane pores opened by the electric stimulus, the location(s) of pore formation on the cell plasma membrane and the lifetime of these pores.

In contrast to "classic" electroporation, the first experimental studies that employed dye uptake assays in cells exposed to ultrashort electric pulses (USEPs, <1 μs pulse duration) reported a lack of dye uptake and, consequently, lack of plasma membrane disruption (Beebe et al. 2003a, b; Pakhomov et al. 2004; Tekle et al. 2005; Vernier et al.

2003, 2004). This observation led to a conclusion that USEPs can bypass cell plasma membrane and affect intracellular structures directly (Schoenbach et al. 2001, 2002, 2007). The possibility of electroporation of organelles by USEPs was generally supported by theoretical models (Gowrishankar and Weaver 2006; Hu et al. 2005; Kotnik and Miklavcic 2006; Smith and Weaver 2008); however, it was also suggested that the plasma membrane should not be "exempt" from poration. Instead, the anticipated effect was formation of relatively small pores in large quantities.

Indeed, patch-clamp measurements in individual cells exposed to USEPs established a profound, long-lasting increase of plasma membrane ionic conductance following USEP exposure (Ibey et al. 2009; Pakhomov et al. 2007a, b, 2009). Plasma membrane permeabilization by USEPs also was visualized using YO-PRO-1 dye instead of PI (Vernier et al. 2006). As a matter of fact, sufficiently intense USEP treatments could trigger PI uptake as well (Pakhomov et al. 2009; Vernier et al. 2006), but it was very modest compared to "typical" dead or electroporated cells (that is why this effect was missed in earlier studies).

Univalent ions that served as charge carriers in the patch-clamp measurements, as well as the YO-PRO-1 dye molecule, are substantially smaller than propidium cation (Fig. 1). (In water solutions, PI [$C_{27}H_{34}N_4I_2$] dissociates into a propidium cation and iodide anions. Nonetheless, numerous publications traditionally use the terms "PI emission" and "PI uptake." However, it is the size of the propidium cation, not of the entire PI molecule, that limits passage of this dye through membrane pores. Hence, below we will mostly use the more accurate terms "propidium emission" and "propidium uptake."). Thus, the experimental data supported the prediction of theoretical models that USEP-opened membrane pores are relatively small.

Assuming that it was indeed the size of the propidium cation that limited its penetration into USEP-treated cells, one can estimate the pore diameter. In the simplest scenario, to prohibit propidium passage, the maximum diameter of a pore should not exceed any two out of three orthogonal dimensions of the propidium molecule. Based on van der Waals dimensions of propidium (Fig. 1) but disregarding any hydration layers (which are too difficult to estimate [Hille 2001] and are beyond the scope of this study), the maximum diameter of a propidium-impermeable pore can be estimated at about 1.5 nm. The diameter of pores formed by conventional electroporation using micro- and millisecond pulses is estimated to fall within the 1–100 nm range (Neumann et al. 1989; Saulis 1999; Saulis et al. 1991). Hence, pores opened by USEPs represent the smallest-sized pore population and were named "nanopores" (Pakhomov et al. 2009; Vernier et al. 2006), to distinguish them from "regular" propidium-permeable electropores of larger diameter.

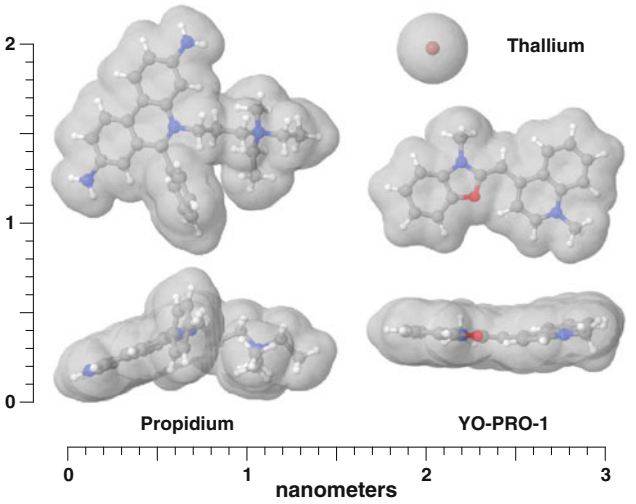

Fig. 1 Relative dimensions of propidium, YO-PRO-1 and thallium cations. Molecular views in two perpendicular planes were generated using Jmol open-source Java viewer for chemical structures in 3D (http://www.jmol.org/). *Gray areas* show van der Waals surface of impenetrable molecular volume (Creighton 1993). The scale is defined by vertical and horizontal rulers

When a modest propidium entry was observed after USEP, it could be explained by thermal fluctuations of nanopore diameter, by formation of a small population of larger pores by fusion of nanopores, or as a sign of nanopore evolution into larger pores as the cell degrades after the USEP insult. One way or another, propidium uptake obviously was not a proper tool for nanopore detection and analysis. Assays with smaller dye molecules like YO-PRO-1 would be a better choice; still, they are likely to miss a significant fraction of the nanopore population with less than ~1 nm diameter.

To solve this problem, we recently introduced fluorescent detection of Tl^+ uptake as a fast and sensitive nanopore detection technique (Pakhomov et al. 2009). Cells were preloaded with FluxOR™ dye (Invitrogen, Eugene, OR), which greatly increases fluorescence in the presence of Tl^+. Since Tl^+ cation is not found in living cells in any appreciable amount, its detection always indicates Tl^+ entry through the plasma membrane (in contrast, e.g., to Ca^{2+}, which can come into the cytosol from intracellular depots). Van der Waals diameter of Tl^+ is only 0.392 nm, which is substantially smaller than any fluorescent dye molecules (Fig. 1) and smaller than Ca^{2+} (0.462 nm). Furthermore, because of its single charge, hydrated Tl^+ is smaller than hydrated Ca^{2+}, and its hydration energy is smaller as well.

In this study, we explored nanopore formation, properties and lifetime using the Tl^+ uptake detection assay. Concurrently, we refined the assay itself and explored its

capabilities in comparison with YO-PRO-1 and propidium uptake methods.

Methods

Cell Cultures and Propagation

In this study, we used three mammalian cell lines: GH3 (murine pituitary), CHO-K1 (Chinese hamster ovary) and NG108 (murine neuroblastoma-rat glioma hybrid). The cells were obtained from ATCC (Manassas, VA) and propagated at 37°C with 5% CO_2 according to the supplier's recommendations. GH3 cells were cultured in Ham's F12K medium supplemented with 2.5% fetal bovine serum (FBS) and 15% horse serum. CHO cells were propagated in Ham's F12K medium supplemented with 10% FBS. NG108 was cultured in Dulbecco's modified Eagle medium without sodium pyruvate, supplemented with 4 mM L-glutamine, 4.5 g/l glucose, 10% FBS, 0.2 mM hypoxanthine, 400 nM aminopterin and 0.016 mM thymidine. The media also contained 1% penicillin/streptomycin. For the passage immediately preceding experiments, cells were transferred onto glass coverslips pretreated with poly-L-lysine to improve cell adhesion.

Cell Imaging

A coverslip with cells was placed into a glass-bottomed chamber (Warner Instruments, Hamden, CT) mounted on an IX71 inverted microscope equipped with an FV 300 confocal laser scanning system (Olympus America, Center Valley, PA). In most experiments, we acquired time series of fluorescent images in parallel with differential-interference contrast (DIC) images using either 40× dry objective (NA 0.95) or 60× oil objective (NA 1.42). All experiments were performed at a room temperature of 22–24°C.

For real-time imaging of Tl^+ uptake, cells were loaded with a Tl^+-sensitive fluorophore (FluxOR Thallium Detection Kit, Invitrogen). Compositions of different test buffers that were used in this study are given in Table 1. When needed, PI and/or YO-PRO-1 were added to the test buffers at concentrations of 30 μg/ml (~50 μM) and 5 μM, respectively. Addition of PI to thallium-containing buffers caused precipitation of insoluble thallium crystals, which were removed by syringe filtering. In some experiments, the buffer was continually flown through the bath, and the flow was switched to a different buffer at predetermined time intervals using a VC-6 valve controller system (Warner Instruments).

The osmolality of all solutions was 290–310 mOsm/kg as measured with a freezing point micro-osmometer (Advanced Instruments, Norwood, MA). Chemicals were purchased from Sigma-Aldrich (St. Louis, MO) and Invitrogen.

FluxOR and YO-PRO-1 were excited with a blue laser (488 nm), and emission was detected in the band from 510 to 530 nm. Due to the similarity of both the emission and excitation spectra, these dyes could only be used

Table 1 Ionic composition of buffers

Buffer	Description	Na^+	K^+	Cs^+	Tl^+	Ca^{2+}	Mg^{2+}	Cl^-	SO_4^{2-}	Glu	Ace	HEPES	TEA	4-AP	EGTA	Figures
1	Complete buffer (CB) for general use, no Tl^+	135	5			2	4	152				10				5a
2	Complete buffer with 16 Tl^+ and K^+-channel blockers (Tl-CB)			70	16	2	2		10		122	10	50	5		3b, 4, 5b, 6, 7, 9
3	Same as 2 but zero Ca^{2+}			70	16		4		12		115	10	50	5	5	7
4	Same as 3 but without K^+ channel blockers			125	16		4		12		120	10			5	7
5	Same as 4 but Na^+ instead of Cs^+	125			16		4		12		120	10			5	7, 8
6	Same as 5 but without Tl^+	137					4		4		132	10				8
7	Same as 4 but with gluconate	127			16		4		12	122		10			5	3a

All concentrations are in millimoles. In addition to listed components, all buffers contained 10 mM of glucose. Final osmolality of all solutions was 290–310 mOsm/kg; pH was adjusted to 7.4 with the base of the respective major cation

Buffers could also contain PI and YO-PRO-1 dye. PI was added as 1 mg/ml stock solution in water, to a final concentration of 30 μg/ml. YO-PRO-1 was added as 1 mM solution in DMSO, to a final concentration of 5 μM

Glu gluconate, *Ace* acetate, *HEPES* 4-(2-hydroxyethyl)piperazine-1-ethanesulfonic acid, *TEA* tetraethylammonium, *EGTA* ethylene glycol-bis (2-aminoethylether)-*N*,*N*,*N*′,*N*′-tetraacetic acid, *4-AP* 4-aminopyridine, *DMSO* dimethyl sulfoxide

separately, in different cell samples. In contrast, propidium (excitation 543 nm laser, emission above 605 nm) could be combined with either of the former two dyes with essentially no "cross-talk."

For revealing propidium and YO-PRO-1 uptake, the fluorescence detector was biased toward maximum sensitivity so that the noisy fluorescent background of the dye-containing bath buffer became visible. These settings facilitated the detection of minimum dye uptake, which would likely be missed when using devices that are factory-preset for cell survival analysis using PI and/or utilize low-NA optics (e.g., flow cytometers, automated cell counters). However, the drawback of these settings was rapid detector saturation if the dye uptake was more than just a minimum value.

In contrast, the sensitivity of the detector for revealing Tl^+ uptake was set at an intermediate level, to avoid saturation even at the maximum signal intensity and to enable "dose–response"-type measurements.

Images were quantified using MetaMorph v. 7.5 (MDS, Foster City, CA). The quantitative data are presented in graphs as mean values ± SE.

Nanosecond Pulse Stimulation and Local Electric Field Modeling

The method of USEP exposure was essentially the same as described recently (Pakhomov et al. 2009). Nearly rectangular 600-ns pulses were generated in a transmission line-type circuit, by closing a MOSFET switch (DE275-102N06A). The amplitude of USEP generated in this transmission line and measured across a matched 50 Ω load was one-half of the charging voltage; these measurements were performed using a 500-MHz Tek P6139A probe connected to a 5-GHz TDS 3052 oscilloscope (Tektronix, Beaverton, OR). For accurate synchronization of USEP exposures with cell image acquisition and bath buffer exchange, all of these processes were triggered externally by a TTL pulse protocol using Digidata 1322A board and pClamp v. 10 software (MDS). When applying multiple USEPs, they were delivered at a rate of 2/s.

USEPs were delivered to a selected cell with a pair of tungsten rod electrodes (0.1 mm diameter, 0.16–0.2 mm gap). With the help of a robotic manipulator (MP-225; Sutter, Novato, CA), these electrodes were positioned precisely at 50 μm above the coverslip surface so that the selected cell was in the middle of the gap between their tips. The electric field at the cell location between the electrodes was determined by 3D simulations with the finite-element Maxwell equation solver Amaze 3D (Field Precision, Albuquerque, NM). The calculations use a Laplace equation and are based on an electrostatic model (either dielectric or conductive). For bath buffer resistivity on the order of 100 ohm × cm, a dielectric relaxation time would be on the order of 1 ns. Since the USEP duration (600 ns) was much greater than the relaxation time, we used the conductive model. A closed, grounded boundary using the Dirichlet condition was set 10 times gap distance away from the USEP-delivering electrodes. The grid size was chosen at 1 or 2 μm, and the accuracy of calculations was verified by comparing the modeled electric field with an analytical solution for a canonical electrode configuration (a two-cylinder electrode submerged in the bath buffer medium).

Results

Tl^+ Uptake is a Sensitive Indicator of Membrane Disruption

The three cell lines employed in this study were chosen for their morphological and physiological diversity. GH3 cells are the smallest (10–12 μm) and always round-shaped (10–12 μm); CHO and NG108 cells are irregularly shaped and much larger (15–30 and 20–50 μm, respectively; Fig. 2). Larger cells are generally regarded as more vulnerable to conventional electroporation with micro- and millisecond pulses; however, it is not known if this holds true for nanosecond pulses as well.

Physiologically, CHO cells are known for very limited expression of endogenous ion channels (Gamper et al. 2005) and typically display no voltage-sensitive currents. In contrast, GH3 and NG108 cells express numerous plasma membrane channels, including voltage-sensitive

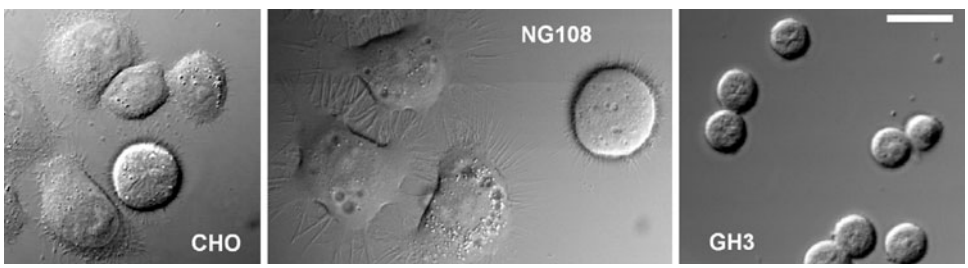

Fig. 2 Comparative dimensions and shapes of three cell types used in Tl^+ uptake studies. Images were taken using DIC optics. Scale bar = 20 μm for all images

Na^+ and Ca^{2+} channels, transient and delayed rectifying K^+ channels and multiple Ca^{2+}-sensitive K^+ channel subtypes (Czarnecki et al. 2003; Stojilkovic et al. 2005; Wu et al. 2009). It is not known yet whether the presence or activation of the ion channels might affect cell permeabilization by USEP or Tl^+ uptake.

In particular, Tl^+ was shown to pass through at least some types of K^+ channels (Niswender et al. 2008; Titus et al. 2009; Weaver et al. 2004), so Tl^+ uptake by activation of voltage-sensitive K^+ channels by USEPs in GH3 and NG108 cells could not be immediately excluded. On the other hand, these studies looked at Tl^+ accumulation in cells over a significant time interval and using a microplate reader; the amount of Tl^+ that would enter the cell by brief opening of K^+ channels may be too small for fluorescent microscopic detection. Nonetheless, to minimize the possibility of K^+ channel involvement, the buffer that was used in most experiments (Table 1, buffer 2, Tl-CB) contained wide-range of K^+ channel inhibitors at concentrations sufficient for complete block of the target channels (DeCoursey et al. 1985). Tl-CB was also used in CHO cells that do not have voltage-gated K^+ channels, just to produce the experimental conditions identical with the other cell lines.

Of note, TlCl has limited solubility in water (<5 mM). To maximize the sensitivity of the assay, we utilized buffers containing 16 mM of Tl^+, so Cl^- was replaced with other anions.

The experiments established fast, dose-dependent uptake of Tl^+ in all tested types of cells (Figs. 3, 4). Typically, Tl^+-dependent emission increased steeply after the USEP and then gradually faded due to bleaching. Triggering any detectable propidium uptake required much higher USEP intensity (either a higher number or amplitude of pulses) and the response usually was delayed.

Consistent with earlier findings (Vernier et al. 2006), comparisons of propidium and Yo-PRO-1 uptake after USEP showed higher sensitivity and greater response of the latter (Fig. 5). However, even Yo-PRO-1 did not detect membrane permeabilization at low USEP intensities, which caused profound Tl^+ uptake (e.g., compare Figs. 4 and 5a). Overall, the sensitivity of the membrane integrity assays decreased with increasing dimensions of the test molecule (Fig. 1), although the dimensions may not be the only factor involved.

Use of Tl^+ Uptake for Quantification of Membrane Permeabilization

The experiments described above suggested that measuring Tl^+ uptake could be a convenient and sensitive technique to evaluate the extent of plasma membrane disruption by USEPs. Such a quantitative approach could be very useful to compare the efficiency of different physical parameters of USEPs (pulse duration, amplitude, number of pulses) and to compare the USEP sensitivity of different cell lines and under different environmental conditions (buffer composition, temperature).

Figure 6a shows the mean normalized response of CHO cells to a single 600-ns pulse applied at various electric field amplitudes. At any intensity that exceeded the permeabilization threshold (1.35–2.1 kV/cm), USEPs caused an immediate surge of fluorescence proportionally to the electric field. In Tl^+-free solutions, USEPs did not change or slightly decreased the fluorescence intensity (e.g., see Fig. 8), so the observed surge in fluorescence was indeed caused by Tl^+ uptake. Note that increasing the electric field had a dual effect, increasing both the rate of initial Tl^+ entry and the steady-state level that was reached 1–2 min after USEP. During the first 6–10 s after the pulse, the emission increased linearly and the slope of the best-fit linear function was employed as a quantitative measure of membrane permeabilization (Fig. 6b). Interestingly, this slope itself (i.e., the initial rate of Tl^+ uptake) also increased linearly with increasing the field intensity, in both CHO and GH3 cells (Fig. 6b). Consistent with earlier reported electrophysiological data (Ibey et al. 2009), GH3 cells were somewhat more sensitive to USEPs than CHO cells, and the threshold electric field for both cell lines was between 1 and 2 kV/cm. Overall, the Tl^+ uptake assay was practically as sensitive as patch-clamp measurements and produced well-matching results.

The measurements summarized in Fig. 6 are time- and labor-intensive (20–35 cells of each type for each electric field level), so we did not perform such a detailed study in NG108 cells. However, the data shown in Fig. 3 suggest a similar electric field threshold for NG108 as for the other cell lines. Within the accuracy of our measurements, very different linear dimensions and shapes of cells (Fig. 2) as well as differences in their physiology played little role in their permeabilization to Tl^+ by 600-ns electric pulses.

Role of the Bath Buffer Composition

In the next series of experiments, we tested if the components of Tl-CB, such as Ca^{2+} and inhibitors of K^+ channels, were really necessary and significantly affected the cell response to USEPs. We found that in CHO cells: (a) replacement of the external Ca^{2+} with Mg^{2+}, (b) removal of TEA^+ and 4-AP and (c) replacement of the external Cs^+ with Na^+ did not change or, unexpectedly, even decreased Tl^+ uptake in comparison with Tl-CB (Fig. 7).

When Ca^{2+} is present in the bath buffer like Tl-CB, one can expect that its entry through nanopores may cause a variety of secondary Ca^{2+}-mediated responses. The fact that the USEP-induced Tl^+ uptake only modestly changed

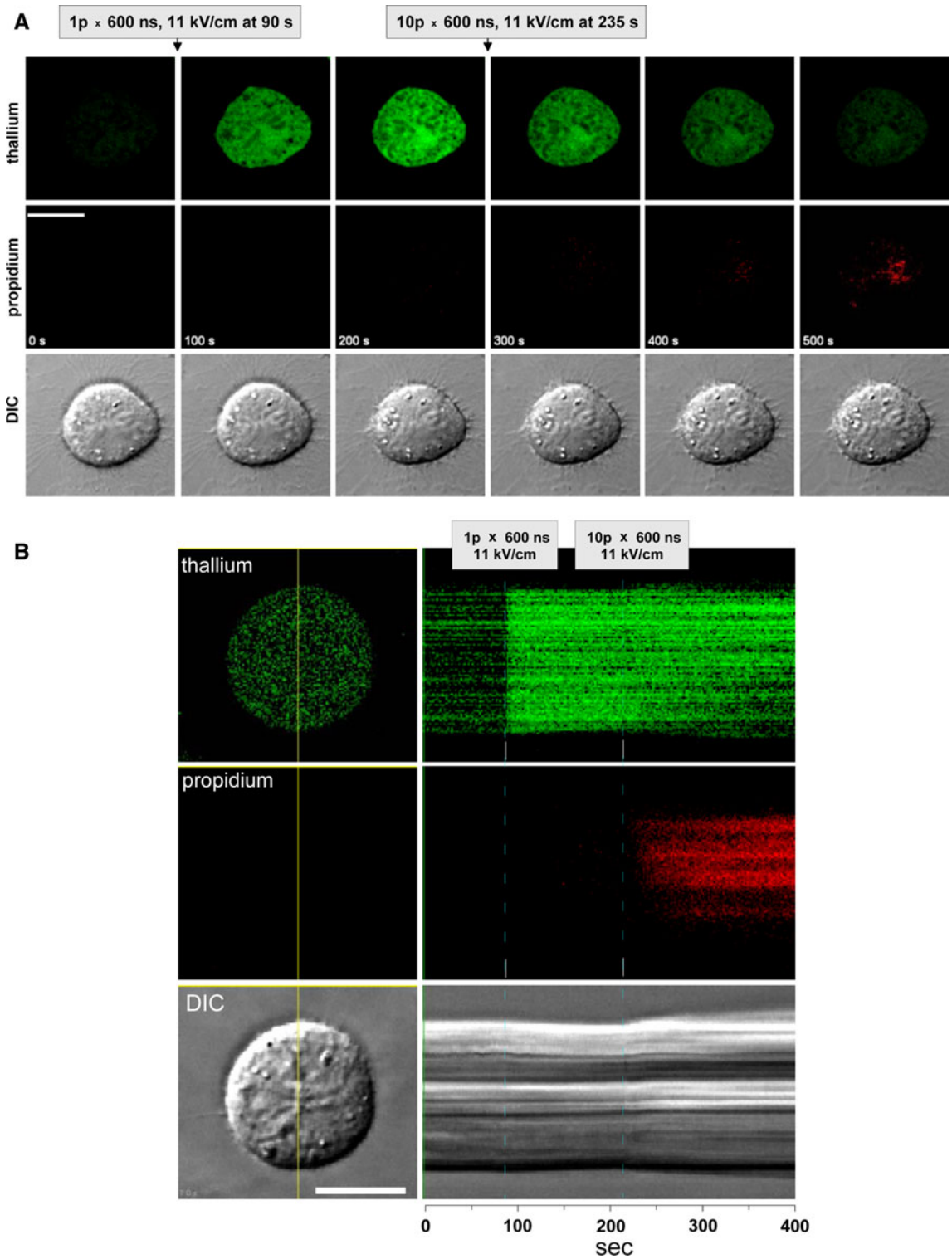

Fig. 3 Concurrent detection of Tl^+ and propidium uptake triggered by USEP exposures. In both **a** and **b**, three rows (*from top to bottom*) are Tl^+-sensitive FluxOR dye emission, propidium emission and DIC images of CHO cells. Images were taken every 2 s. **a** Selected image triplets at indicated times from the start of the experiment. **b** *Left panels* Cell images at the onset of the experiment. *Line drawn over the images* denotes the position of an imaginable "slice" through the time lapse stack of 2D images. *Right panels* This "slice" as a time change display; i.e., they show how the image at the position of the line changed over time. The parameters of two USEP exposures are shown at the top; *1p* and *10p* correspond to one pulse and a train of 10 pulses, respectively. **b** Onset of exposures is shown by *vertical dashed lines* over the time change display. Note fast and profound uptake of Tl^+ after a single pulse but only a weak and delayed uptake of propidium after 10 pulses. Bath buffers were 7 (**a**) and 2 (**b**), see Table 1. Scale bars = 10 μm

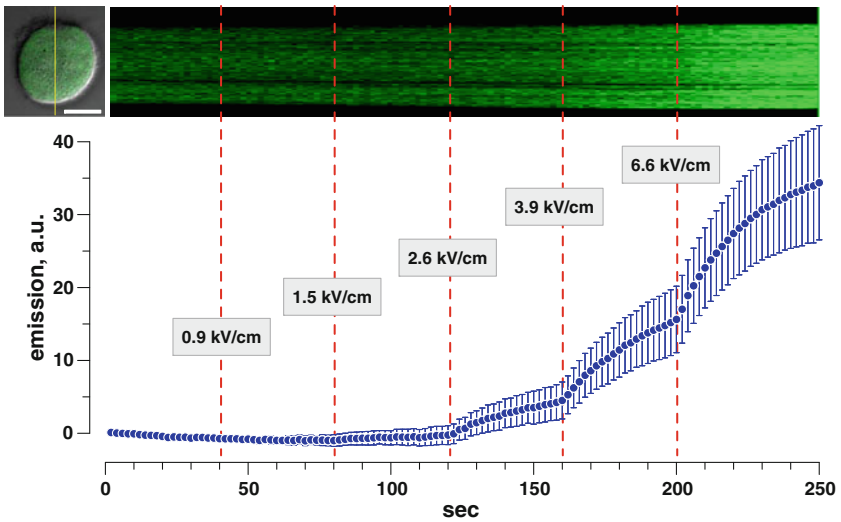

Fig. 4 Effect of sequential USEP exposures at increasing intensity on Tl^+ uptake in NG108 cells. The intensity of FluxOR dye emission was measured every 2 s in three neuroblastoma cells in buffer 2 (Table 1). *Vertical dashed lines* show times of single-pulse exposures at indicated intensities. *Inset* Overlapped fluorescent and DIC images of one of the cells and a respective time change display of fluorescence (see Fig. 3b for detail). Scale bar = 10 µm. Note stepwise emission increases in response to USEP exposures, with the threshold between 1.5 and 2.6 kV/cm

in Ca^{2+}-free bath buffers is consistent with the concept of plasma membrane permeabilization as a direct and immediate effect of USEPs (rather than a secondary effect mediated by intracellular cascades). Likewise, the fact that removal of K^+ channel blockers did not increase the rate or amplitude of Tl^+ uptake indicates that the endogenous K^+ channels played little or no role in this process. Moreover, removal of Ca^{2+} and K^+ channel blockers decreased the USEP-induced Tl^+ uptake. One can speculate that, for example, increasing of the bath concentrations of Na^+ or Cs^+ (instead of removing larger molecules of TEA^+ and 4-AP) could increase competition with Tl^+ for nanopore entry; however, the exact causes of this effect remain unclear.

Most importantly, these experiments demonstrated that nanopore-mediated Tl^+ uptake can be reliably and reproducibly observed under various bath buffer conditions, thereby making it possible to employ this assay in diverse pharmacological and physiological studies of nanopore formation, conductance and resealing.

Testing for Nanopore Lifetime

Previous studies using patch clamp demonstrated that the USEP-induced increase of membrane conductance persists at room temperature for as long as 10–15 min after treatment (Pakhomov et al. 2007a). The Tl^+ uptake assay can be employed as an independent and noninvasive technique to verify the electrophysiological findings. To do so, FluxOR-loaded cells are placed in the flow of a Tl^+-free bath buffer and subjected to USEP stimulation. At a certain interval after USEP, the solution flow is switched to a buffer that contains Tl^+. If nanopores remain open by the time of buffer switching, the fluorescence sharply increases due to Tl^+ entry into cells. This protocol was tested recently in CHO cells using a Tl^+-free version of Tl-CB (Tl^+ replaced with an equimolar amount of Cs^+) followed by Tl-CB superfusion, and the data confirmed that the lifetime of nanopores is on the order of minutes (Pakhomov et al. 2009).

Here, we report the results of a more comprehensive experiment done in NG108 cells and using a different combination of Tl^+-free and Tl^+-containing buffers (Fig. 8). For this particular combination of buffers, switching to the Tl^+-containing buffer caused a gradual increase in fluorescence even in cells that were not exposed to USEPs (Fig. 8, lower graphs). This uptake could occur by endocytosis or via some constitutively open endogenous ion channels; the time course and magnitude of this Tl^+ uptake did not depend on the time interval after sham exposure. (Notably, the "spontaneous" Tl^+ uptake was much weaker or completely absent when using the other Tl^+-containing buffers listed in Table 1; e.g., see Figs. 3b, 4, 7.)

The same switching of the buffers shortly after exposure to one 600-ns pulse at 6.6 kV/cm caused much faster and more profound Tl^+ uptake (Fig. 8, upper graphs). By increasing the time interval between USEPs and Tl^+ delivery, this surge of Tl^+ uptake gradually tapered out and reached the control level by 600 s after exposure.

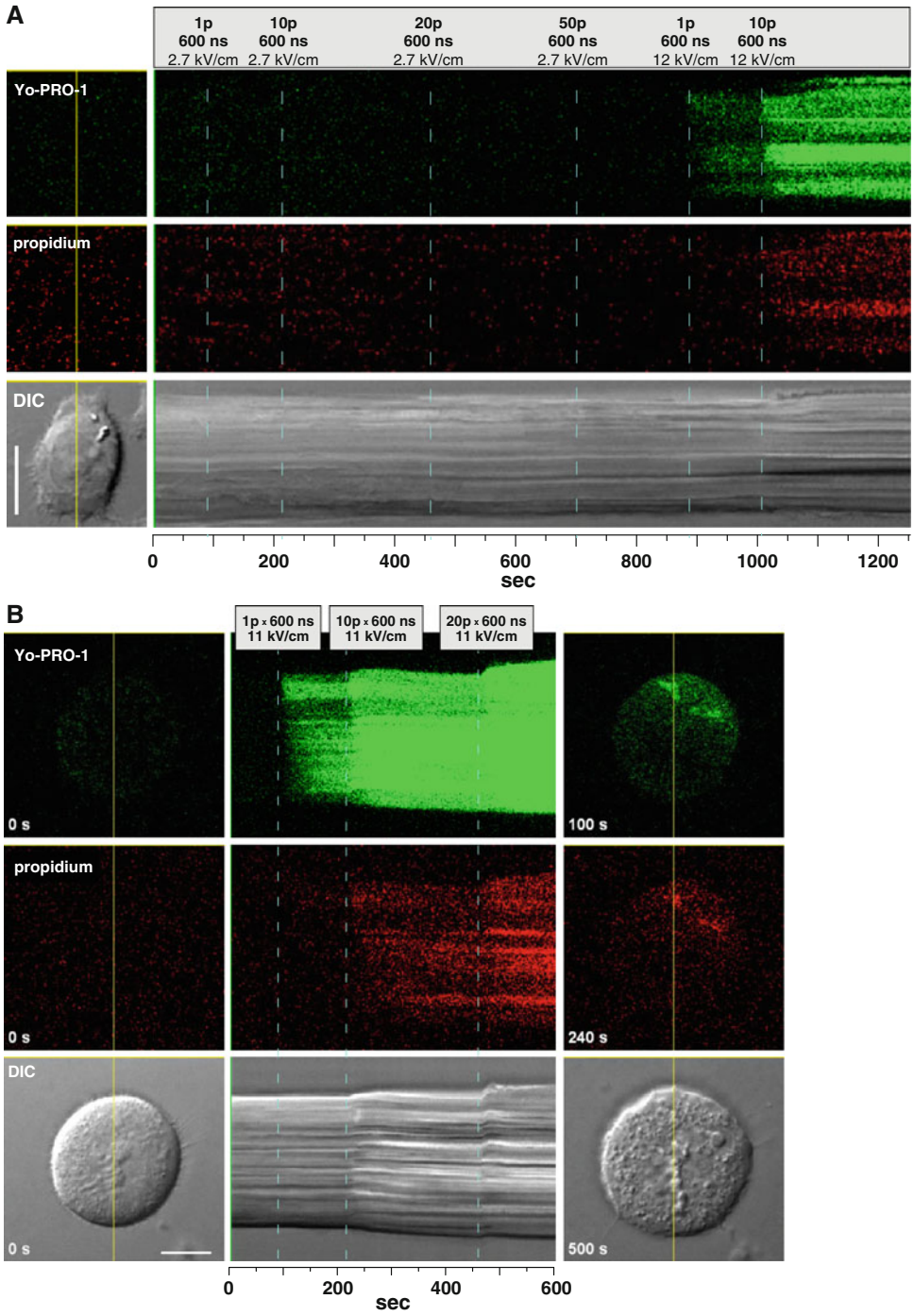

Fig. 5 Concurrent detection of YO-PRO-1 and propidium uptake triggered by USEP exposures in CHO cells. Images were prepared the same way as in Fig. 3b, but the *top row* is YO-PRO-1 emission. **a** Only 12-kV/cm pulses triggered dye uptake. **b** Additional cell images at *right* show that uptake of both tested dyes started from the right-hand top side of the cell (this was the side facing the positive USEP-delivering electrode, not shown). Bath buffers were 1 (**a**) and 2 (**b**), see Table 1. Scale bars = 20 μm (**a**) and 10 μm (**b**)

Taken together with the previously reported findings (Pakhomov et al. 2007a, 2009), these new data indicate that nanopore lifetime at room temperature is on the order of 10 min in such diverse cell lines as GH3, CHO and NG108. Most interesting, this lifetime was similar in Ca^{2+}-containing and Ca^{2+}-free buffers. The entry of Ca^{2+} is considered to play a key role in triggering active repair of membrane damage by exo- and endocytosis (Idone et al. 2008a, b). In our experiments, the lack of Ca^{2+} effect on nanopore resealing could be indicative of the fact that cells exposed to low-intensity USEPs remained impermeable to Ca^{2+}. Indeed, exposure of Jurkat cells to 60-ns pulses triggered Ca^{2+} entry at 100 kV/cm but not at 50 kV/cm (Scarlett et al. 2009). Using the absorbed dose to compare USEP efficiency at different pulse durations (Ibey et al. 2009) and assuming similar conductance of the pulsing

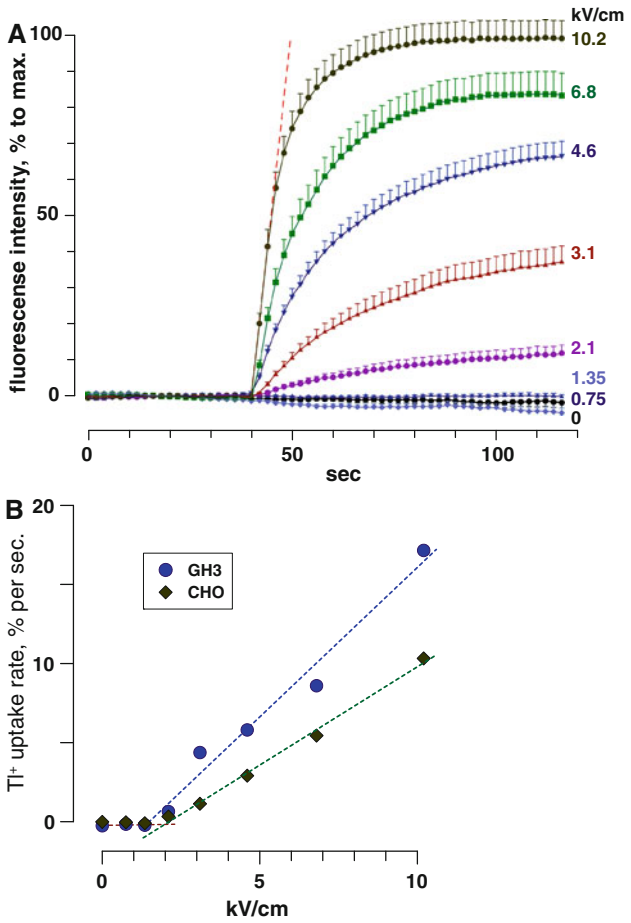

Fig. 6 Membrane permeabilization by USEPs at different electric field intensities as quantified by Tl^+ uptake. **a** CHO cells were bathed in Tl-CB (buffer 2, Table 1), and fluorescent images were taken every 2 s. A single 600-ns pulse was applied at 40 s; the electric field intensity is indicated to the *right* of the graphs (20–35 cells from 5–10 independent experiments per each condition). For clarity, error bars are shown in one direction only. The initial (pre-exposure) emission value was taken as zero, and the mean steady-state emission value after the most intense exposure (10.2 kV/cm) was taken as 100%. Note that the initial rise in fluorescence intensity immediately after USEP was practically linear; for clarity, the best-fit linear function is shown for 10.2 kV/cm exposure only (*dashed line*). The slope of this line reflects the initial rate of Tl^+ uptake and was used in **b** as a measure of membrane permeabilization. The original data for GH3 cells are not shown but are similar to those for CHO cells in **a**. Note that the rate of Tl^+ uptake increased almost linearly with increasing electric field, with the threshold for both cell lines between 1 and 2 kV/cm

buffers, 100 kV/cm at 60-ns pulse duration corresponds to 33 kV/cm at 600 ns, which is much higher than the 6.6 kV/cm that we used.

Fast Recording of Tl^+ Uptake

Detection of Tl^+ uptake within a short interval (milliseconds) after USEPs could serve as a strong confirmation that it is indeed a direct effect of USEPs on the membrane, rather than a secondary effect mediated by biological cascades. Using fast image acquisition rates, we saw Tl^+ uptake already during the first scan after USEPs, i.e., within less than 0.05–0.1 s after the pulse (Fig. 9). Experiments in CHO and NG108 cells yielded similar results. Interestingly, we never observed localized Tl^+ entry from the anodic pole of the cell, which is a well-known effect for propidium and YO-PRO-1 entry (Neumann et al. 1989; Pakhomov et al. 2009; Vernier et al. 2006; see also Fig. 5b). It remains to be seen if still faster image acquisition is needed to reveal polar uptake of this dye or if nanopores may indeed form diffusely over the plasma membrane surface, as suggested by the "supra-electroporation" model (Gowrishankar and Weaver 2006).

Discussion

Cell membrane permeabilization with high-amplitude, micro- and millisecond duration pulses has been a subject of intense research for several decades. However, its mechanism is still being debated. Although the formation of aqueous pores by accumulation of charges at the plasma membrane, followed by membrane breakdown, is the most widely accepted mechanism, it does not adequately explain all experimental findings (Teissie et al. 2005).

The terms "nanopore" and "nanoelectroporation" have been introduced only recently, with somewhat ambiguous meaning: They could mean both electroporation by nanosecond-duration electric pulses and formation of pores with diameter of $\sim$ 1 nm. These definitions do not contradict each other, as the application of nanosecond-duration electric pulses (or USEPs) is considered a right tool to open nanometer-diameter membrane pores. Still, we prefer the size-based definition of nanopores, as it applies to these membrane defects regardless of the exact way they were opened.

We used USEPs as a convenient and efficient tool to produce nanopores, but there is little reason to believe that USEPs are the only or unique way of doing it. Depending on exposure conditions, longer electric pulses produce heterogeneous populations of membrane pores, with sizes ranging from $\sim$1 to $\sim$100 nm, so nanopores would be included in this range. Nanopores could also be a brief initial stage of larger pore formation (Glaser et al. 1988). Conversely, larger electropores may shrink to 1–2 nm, producing a relatively stable nanopore population (Saulis 1999). Moreover, nanopores may open in lipid bilayers "spontaneously," without application of an external field (Volkov et al. 1997). We found that nanopores exert complex conductive properties, which are not found in larger electropores (Pakhomov et al.

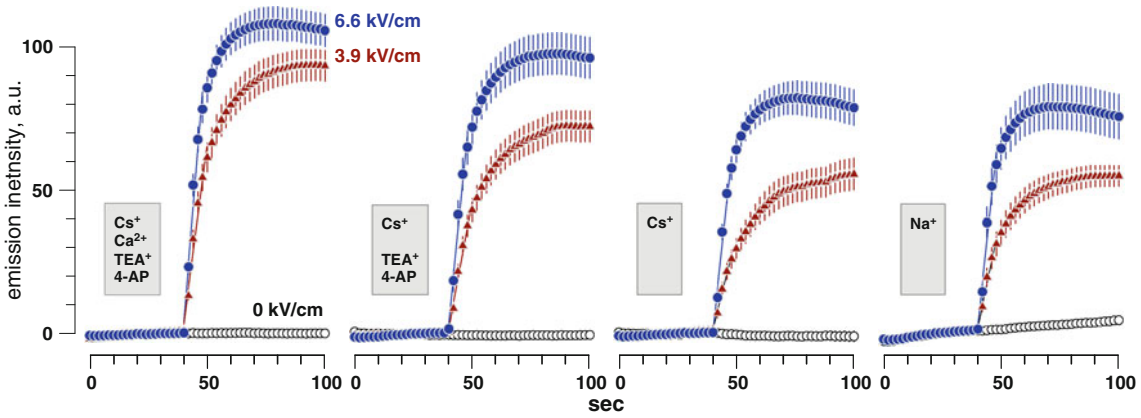

Fig. 7 Effect of bath buffer composition on USEP-triggered Tl^+ uptake. CHO cells were exposed at 40 s to a single 600-ns pulse at 0 (control), 3.9 or 6.6 kV/cm in different buffers (20–30 cells per condition). Bath buffers, *from left to right panels*, were 2, 3, 4 and 5, respectively (see Table 1). Principal changes to buffer composition are outlined in *boxes next to graphs*. In short, buffer 2 (*left panel*) contained Cs^+ and Ca^{2+} ions and K^+-channel blockers TEA and 4-AP. For experiments in the *second panel*, Ca^{2+} was removed from the buffer. *Third panel* TEA and 4-AP were also removed. *Right panel* Cs^+ was also removed and replaced with Na^+

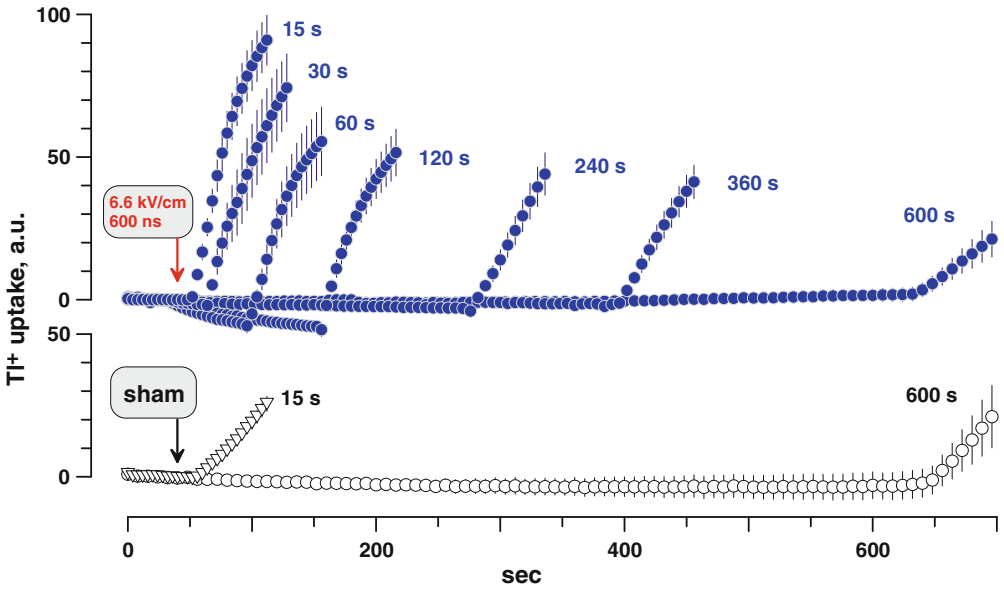

Fig. 8 Timeline of nanopore resealing as visualized by gradual reduction of Tl^+ uptake with time after USEP exposure. NG108 cells were placed in a Tl^+-free buffer (6, Table 1) and subjected to a single 600-ns pulse at either 6.6 kV/cm (*top graphs*) or 0 kV/cm ("sham" exposure, *bottom graphs*); 8–11 cells per group. At indicated time intervals after USEP, the bath perfusion was switched to buffer 5, containing 16 mM of Tl^+. Uptake of Tl^+ caused a surge of cell fluorescence, which was more profound if nanopores were still open. See text for more detail

2009) but resemble those of nonselective cation ion channels, so these channels could have been confused with nanopores in some earlier studies. We concluded that nanopores constitute a distinct transmembrane passageway that plays a significant role in cell function but, as of today, has only been scarcely explored (Pakhomov and Pakhomova 2010).

Indeed, the choice of experimental techniques that could be employed for selective, on-demand triggering of nanopore formation and their functional analyses has been very limited. In this report, we demonstrate that fluorescent detection of Tl^+ uptake by USEP-exposed cells is a novel, highly sensitive and versatile tool for nanopore studies. While patch clamp remains arguably the most informative approach to analyze nanopore currents, the Tl^+ detection method shows similar sensitivity and is fast, noninvasive and far more efficient.

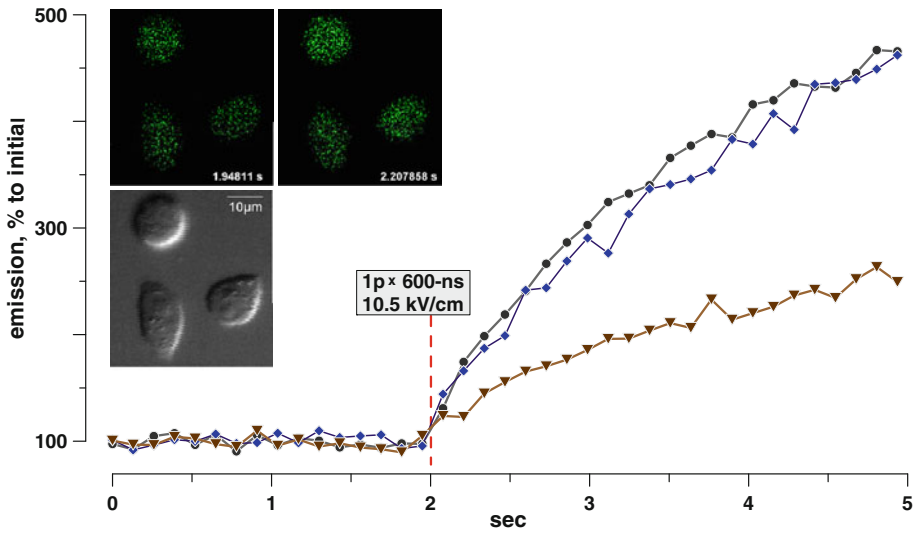

Fig. 9 Fast onset of USEP-triggered Tl^+ uptake. Shown are individual data for three CHO cells (*inset*) bathed in Tl-CB (buffer 2, Table 1). Images were taken every 130 ms, with a scanning time of about 40 ms per image. Note diffuse Tl^+ entry (*inset*), in contrast to single pole entry of other dyes (Fig. 5b). See text for more detail

Acknowledgements The work was supported by R01CA125482 from the National Cancer Institute.

References

Beebe SJ, Fox PM, Rec LJ, Willis EL, Schoenbach KH (2003a) Nanosecond, high-intensity pulsed electric fields induce apoptosis in human cells. FASEB J 17:1493–1495

Beebe SJ, White J, Blackmore PF, Deng Y, Somers K, Schoenbach KH (2003b) Diverse effects of nanosecond pulsed electric fields on cells and tissues. DNA Cell Biol 22:785–796

Creighton TE (1993) Proteins: structures and molecular properties. WH Freeman, New York

Czarnecki A, Dufy-Barbe L, Huet S, Odessa M-F, Bresson-Bepoldin L (2003) Potassium channel expression level is dependent on the proliferation state in the GH3 pituitary cell line. Am J Physiol Cell Physiol 284:1054–1064

DeCoursey TE, Chandy KG, Gupta S, Cahalan MD (1985) Voltage-dependent ion channels in T-lymphocytes. J Neuroimmunol 10:71–95

Djuzenova CS, Zimmermann U, Frank H, Sukhorukov VL, Richter E, Fuhr G (1996) Effect of medium conductivity and composition on the uptake of propidium iodide into electropermeabilized myeloma cells. Biochim Biophys Acta 1284:143–152

Gamper N, Stockand JD, Shapiro MS (2005) The use of Chinese hamster ovary (CHO) cells in the study of ion channels. J Pharmacol Toxicol Methods 51:177–185

Glaser RW, Leikin SL, Chernomordik LV, Pastushenko VF, Sokirko AI (1988) Reversible electrical breakdown of lipid bilayers: formation and evolution of pores. Biochim Biophys Acta 940:275–287

Golzio M, Teissie J, Rols MP (2002) Direct visualization at the single-cell level of electrically mediated gene delivery. Proc Natl Acad Sci USA 99:1292–1297

Gowrishankar TR, Weaver JC (2006) Electrical behavior and pore accumulation in a multicellular model for conventional and supra-electroporation. Biochem Biophys Res Commun 349:643–653

Hille B (2001) Ionic channels of excitable membranes. Sinauer Associates, Sunderland

Hu Q, Viswanadham S, Joshi RP, Schoenbach KH, Beebe SJ, Blackmore PF (2005) Simulations of transient membrane behavior in cells subjected to a high-intensity, ultra-short electric pulse. Phys Rev E 71:031914

Ibey BL, Xiao S, Schoenbach KH, Murphy MR, Pakhomov AG (2009) Plasma membrane permeabilization by 60- and 600-ns electric pulses is determined by the absorbed dose. Bioelectromagnetics 30:92–99

Idone V, Tam C, Andrews NW (2008a) Two-way traffic on the road to plasma membrane repair. Trends Cell Biol 18:552–559

Idone V, Tam C, Goss JW, Toomre D, Pypaert M, Andrews NW (2008b) Repair of injured plasma membrane by rapid Ca^{2+}-dependent endocytosis. J Cell Biol 180:905–914

Kotnik T, Miklavcic D (2006) Theoretical evaluation of voltage inducement on internal membranes of biological cells exposed to electric fields. Biophys J 90:480–491

Neumann E, Sowers AE, Jordan CA (1989) Electroporation and electrofusion in cell biology. Plenum, New York

Niswender CM, Johnson KA, Luo Q, Ayala JE, Kim C, Conn PJ, Weaver CD (2008) A novel assay of Gi/o-linked G protein-coupled receptor coupling to potassium channels provides new insights into the pharmacology of the group III metabotropic glutamate receptors. Mol Pharmacol 73:1213–1224

Pakhomov AG, Pakhomova ON (2010) Nanopores: a distinct transmembrane passageway in electroporated cells. In: Pakhomov AG, Miklavcic D, Markov MS (eds) Advanced electroporation techniques in biology in medicine. CRC Press, pp 178–194

Pakhomov AG, Phinney A, Ashmore J, Walker KJK, Kono S, Schoenbach KS, Murphy MR (2004) Characterization of the cytotoxic effect of high-intensity, 10-ns duration electrical pulses. IEEE Trans Plasma Sci 32:1579–1585

Pakhomov AG, Kolb JF, White JA, Joshi RP, Xiao S, Schoenbach KH (2007a) Long-lasting plasma membrane permeabilization in mammalian cells by nanosecond pulsed electric field (nsPEF). Bioelectromagnetics 28:655–663

Pakhomov AG, Shevin R, White JA, Kolb JF, Pakhomova ON, Joshi RP, Schoenbach KH (2007b) Membrane permeabilization and cell damage by ultrashort electric field shocks. Arch Biochem Biophys 465:109–118

Pakhomov AG, Bowman AM, Ibey BL, Andre FM, Pakhomova ON, Schoenbach KH (2009) Lipid nanopores can form a stable, ion channel-like conduction pathway in cell membrane. Biochem Biophys Res Commun 385:181–186

Saulis G (1999) Kinetics of pore disappearance in a cell after electroporation. Biomed Sci Instrum 35:409–414

Saulis G, Venslauskas MS, Naktinis J (1991) Kinetics of pore resealing in cell membranes after electroporation. Bioelectrochem Bioenerg 26:1–13

Scarlett SS, White JA, Blackmore PF, Schoenbach KH, Kolb JF (2009) Regulation of intracellular calcium concentration by nanosecond pulsed electric fields. Biochim Biophys Acta 1788:1168–1175

Schoenbach KH, Beebe SJ, Buescher ES (2001) Intracellular effect of ultrashort electrical pulses. Bioelectromagnetics 22:440–448

Schoenbach KH, Katsuki S, Stark RH, Buesher ES, Beebe SJ (2002) Bioelectrics—new applications for pulsed power technology. IEEE Trans Plasma Sci 30:293–300

Schoenbach KS, Hargrave B, Joshi RP, Kolb J, Osgood C, Nuccitelli R, Pakhomov AG, Swanson J, Stacey M, White JA, Xiao S, Zhang J (2007) Bioelectric effects of nanosecond pulses. IEEE Trans Dielectr Electr Insul 14:1088–1109

Smith KC, Weaver JC (2008) Active mechanisms are needed to describe cell responses to submicrosecond, megavolt-per-meter pulses: cell models for ultrashort pulses. Biophys J 95:1547–1563

Stojilkovic SS, Zemkova H, Goor FV (2005) Biophysical basis of pituitary cell type-specific Ca^{2+} signaling–secretion coupling. Trends Endocrinol Metab 16:152–159

Teissie J, Golzio M, Rols MP (2005) Mechanisms of cell membrane electropermeabilization: a minireview of our present (lack of?) knowledge. Biochim Biophys Acta 1724:270–280

Tekle E, Astumian RD, Chock PB (1994) Selective and asymmetric molecular transport across electroporated cell membranes. Proc Natl Acad Sci USA 91:11512–11516

Tekle E, Oubrahim H, Dzekunov SM, Kolb JF, Schoenbach KH, Chock PB (2005) Selective field effects on intracellular vacuoles and vesicle membranes with nanosecond electric pulses. Biophys J 89:274–284

Titus SA, Beacham D, Shahane SA, Southall N, Xia M, Huang R, Hooten E, Zhao Y, Shou L, Austin CP, Zheng W (2009) A new homogeneous high-throughput screening assay for profiling compound activity on the human ether-a-go-go-related gene channel. Anal Biochem 394:30–38

Vernier PT, Sun Y, Marcu L, Salem S, Craft CM, Gundersen MA (2003) Calcium bursts induced by nanosecond electric pulses. Biochem Biophys Res Commun 310:286–295

Vernier PT, Sun Y, Marcu L, Craft CM, Gundersen MA (2004) Nanoelectropulse-induced phosphatidylserine translocation. Biophys J 86:4040–4048

Vernier PT, Sun Y, Gundersen MA (2006) Nanoelectropulse-driven membrane perturbation and small molecule permeabilization. BMC Cell Biol 7:37

Volkov AG, Paula S, Deamer DW (1997) Two mechanisms of permeation of small neutral molecules and hydrated ions across phospholipid bilayers. Bioelectrochem Bioenerg 42:153–160

Weaver JC (2000) Electroporation of cells and tissues. IEEE Trans Plasma Sci 28:24–33

Weaver CD, Harden D, Dworetzky SI, Robertson B, Knox RJ (2004) A thallium-sensitive, fluorescence-based assay for detecting and characterizing potassium channel modulators in mammalian cells. J Biomol Screen 9:671–677

Wu SN, Chen BS, Wu YH, Peng H, Chen LT (2009) The mechanism of the actions of oxaliplatin on ion currents and action potentials in differentiated NG108-15 neuronal cells. Neurotoxicology 30:677–685

Zimmermann U, Friedrich U, Mussauer H, Gessner P, Hämel K, Sukhorukov V (2000) Electromanipulation of mammalian cells: fundamentals and application. IEEE Trans Plasma Sci 28:72–82